Disentangling the role of athermal walls on the Knudsen paradox in molecular and granular gases

Ronak Gupta and Meheboob Alam*

Engineering Mechanics Unit, Jawaharlal Nehru Centre for Advanced Scientific Research, Jakkur PO, Bangalore 560064, India

(Received 29 October 2017; published 29 January 2018)

The nature of particle-wall interactions is shown to have a profound impact on the well-known "Knudsen paradox" [or the "Knudsen minimum" effect, which refers to the decrease of the mass-flow rate of a gas with increasing Knudsen number Kn, reaching a minimum at Kn $\sim O(1)$ and increasing logarithmically with Kn as Kn $\to \infty$] in the acceleration-driven Poiseuille flow of rarefied gases. The nonmonotonic variation of the flow rate with Kn occurs even in a granular or dissipative gas in contact with thermal walls. The latter result is in contradiction with recent work [Alam *et al.*, J. Fluid Mech. **782**, 99 (2015)] that revealed the absence of the Knudsen minimum in granular Poiseuille flow for which the flow rate was found to decrease at large values of Kn. The above conundrum is resolved by distinguishing between "thermal" and "athermal" walls, and it is shown that, for both molecular and granular gases, the momentum transfer to athermal walls is much different than that to thermal walls which is directly responsible for the anomalous flow-rate variation with Kn in the rarefied regime. In the continuum limit of Kn $\to 0$, the athermal walls are shown to be closely related to "no-flux" ("adiabatic") walls for which the Knudsen minimum does not exist either. A possible characterization of athermal walls in terms of (1) an effective specularity coefficient for the slip velocity and (2) a flux-type boundary condition for granular temperature is suggested based on simulation results.

DOI: 10.1103/PhysRevE.97.012912

I. INTRODUCTION

Molecular gas flows are generally classified [1–5] based on the Knudsen number (Kn, the ratio between the mean-free path and a characteristic length of the system): (1) the continuum flow if Kn $\leqslant 0.01$, (2) the slip flow if $0.01 <$ Kn $\leqslant 0.1$, (3) the transition flow if $0.1 <$ Kn < 10, and (4) the free molecular flow if Kn $\geqslant 10$. The (2) slip and (3) transition flow regimes are collectively dubbed "rarefied" flows for which the standard Navier-Stokes-Fourier (NSF) equations are known to be inadequate to describe many flow features that are unique to rarefied molecular gases: the Knudsen paradox [2,6], nonzero transverse heat flux [7], normal stress differences [8], and temperature bimodality [9–11].

The present paper deals with the well-known "Knudsen paradox," which refers to the nonmonotonic variation of the mass-flow rate with the Knudsen number for a molecular gas undergoing plane Poiseuille flow as depicted in Fig. 1. The dimensionless mass-flow rate is calculated from

$$Q_T = \frac{1}{\rho_{av} v_w W\left(gW/v_w^2\right)} \int_{-W/2}^{W/2} \rho(y) u_x(y)\, dy, \qquad (1)$$

where $u_x(y)$ is the streamwise component of the hydrodynamic velocity, ρ_{av} is the average density of the gas, g the gravitational acceleration, W is the separation between two walls (see the inset of Fig. 1), and $v_w = \sqrt{2k_B T_w/m}$ is the reference thermal velocity at wall temperature T_w. Figure 1 indicates the flow rate decreases with increasing Kn, reaches a minimum at Kn $= O(1)$, and increases thereafter slowly with further increasing Kn; this nonmonotonic flow-rate variation with Kn is also dubbed the *Knudsen minimum effect*. This phenomenon was discovered by Knudsen [2] experimentally while measuring the mass-flow rate of rarefied gases passing through a capillary tube under different pressure heads. This was indeed a "paradox" since the standard Navier-Stokes equations predict a monotonic decay of the flow rate with increasing Kn, a theoretical resolution of which came after 50 years [6]. Cercignani and Daneri [6] solved the Bhatnagar-Gross-Krook (BGK)-Boltzmann equation for rarefied gases, and their asymptotic analysis revealed that the decrease of the flow rate is linear,

$$Q \sim \mathrm{Kn}^{-1} \quad \text{at} \quad \mathrm{Kn} \sim 0, \qquad (2)$$

but increases logarithmically,

$$Q \sim \log \mathrm{Kn} \quad \text{at} \quad \mathrm{Kn} \to \infty, \qquad (3)$$

with its minimum occurring at Kn $\sim O(1)$. Although the original experiments by Knudsen correspond to the "pressure-driven" Poiseuille flow of rarefied gases, the acceleration-driven Poiseuille flow [12] is equivalent to its classical pressure-driven counterpart [13,14] (as long as the dimensionless acceleration, $\widehat{g} = gW/v_w^2$, is small such that the flow remains in the low Mach number regime) as demonstrated in Fig. 1, and the basic features of Knudsen minimum effect remain unchanged irrespective of whether the flow is driven by an imposed pressure gradient or a body force [4,15].

Moving to dissipative or granular gases [16–18], the Knudsen minimum effect was studied by Alam *et al.* [19] for the first time for a granular gas via molecular dynamics (MD) simulations of the gravity-driven Poiseuille flow of inelastic hard disks. Their results revealed that the Knudsen minimum is absent in a granular or dissipative gas, except in the singular case of nearly elastic particles flowing through a channel

*meheboob@jncasr.ac.in

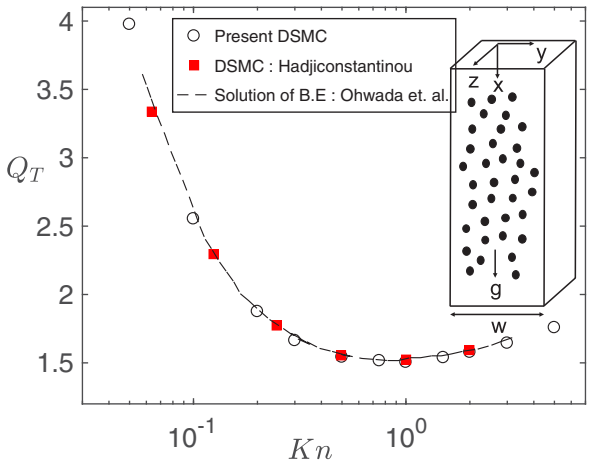

FIG. 1. Mass flow rate [Eq. (1)] versus Knudsen number (Kn) for a molecular gas: the results from present direct simulation Monte Carlo (DSMC) code (circles) are compared with previous simulation (red squares [12]) and the solution of the Boltzmann equation (dashed line [13]); see text for details. The dimensionless acceleration is set to $\widehat{g} = mgW/2k_BT_w = 0.05$. Inset: a sketch of acceleration-driven Poiseuille flow.

bounded by "smooth" walls (described in Sec. II B) for which both a local minimum and a maximum in the flow rate were found to occur at finite values of Kn; see Fig. 2. Moreover, for dissipative particles ($e_n < 0.98$), the flow rate was found to decrease monotonically with increasing Kn as confirmed in the inset of Fig. 2. Overall, irrespective of the choice of the wall roughness and the restitution coefficient, the flow rate at sufficiently large values of Kn is found to decrease with increasing Kn [19]; this implies that the well-known logarithmically increasing branch [Eq. (3)] is absent in Poiseuille flow in contact with athermal walls. The results of

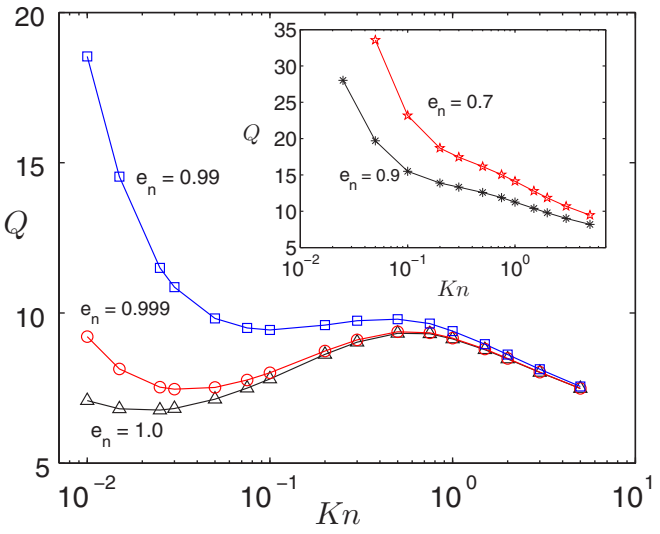

FIG. 2. Dimensionless mass-flow rate [Eq. (12)] versus Knudsen number for different e_n in channels with nearly "smooth walls" $\beta_w = -0.9$ (see Sec. II B on the definition of "athermal" walls); inset shows results for $e_n = 0.9$ and 0.7.

Alam *et al.* [19] are, therefore, in contradiction to the well-studied Knudsen-paradox (Fig. 1) in molecular gases. On the other hand, our recent work [20] with "fully diffuse" thermal walls [using the direct-simulation Monte Carlo (DSMC) method [21]] confirmed that the "logarithmically increasing branch" [Eq. (3)] survives in granular gases too. The walls being thermal or athermal seems to be playing a crucial role on the overall flow rate in the rarefied regime (Kn $\gg$ 1), and the resolution of this conundrum forms the main motivation of the present paper.

In this work our focus is to analyze and understand the roles of particle-wall interactions and inelasticity on the Knudsen minimum effect; this eventually helps to disentangle the roles of different wall conditions on the flow-rate variation and the origin of Knudsen paradox. As in Ref. [20] we use the DSMC method to simulate the grains flowing under the action of gravity between two parallel walls which are modeled as "thermal" (Sec. II A) and "athermal" (Sec. II B) walls. The distinction between thermal and athermal walls turns out to be crucial since we find (Sec. III) that the walls being thermal or athemal can be tied to the existence or absence of the Knudsen minimum. A broader class of wall conditions is then analyzed which suggests that the Knudsen minimum can also disappear in a molecular gas if the "adiabatic" wall conditions (Sec. III C) are imposed. The presence or absence of the logarithmically increasing branch [Eq. (3)] is discussed in Sec. IV, with reference to the effective momentum transfer to walls due to particle-wall collisions.

II. THERMAL AND ATHERMAL WALL CONDITIONS

For particle-wall collisions, the postcollision velocities are assigned in accordance with the type of wall employed: *thermal* and *athermal* walls as discussed below.

A. Thermal walls: Diffuse and specular collisions

In the DSMC method, the simulation particles are treated as physical particles to specify boundary conditions. A "thermal" wall [20,22] can be imagined as a boundary connected to a heat reservoir at a certain temperature, and the wall is assumed to be in thermal equilibrium with the reservoir. A gas molecule hitting the wall forgets its initial velocity and is reemitted from the wall having adopted the wall temperature with zero average tangential velocity; this refers to the original "diffuse" wall condition of Maxwell [1]. On the other hand, for "specular-type" particle-wall collisions, the tangential component of the particle velocity remains unchanged, but only its normal component gets reversed, resulting in zero exchange of tangential momentum between fluid particles and the wall.

Here we use a mixed model [4] that incorporates both "specular" and "diffuse" collisions: a fraction of α particles is diffusely reflected from the wall (maintained at T_w), and the remaining fraction of $(1-\alpha)$ particles undergoes specular collisions. For "'diffuse" particle-wall collisions, the postcollisional velocities are chosen as follows [20,23]:

$$v_x^{t+\Delta t} = \sqrt{\frac{k_B T_w}{m}}\, v_M + g t_{\text{post}}, \tag{4}$$

$$v_y^{t+\Delta t} = sgn(\widehat{n}_w)\sqrt{\frac{2k_BT_w}{m}}v_{BM}, \tag{5}$$

$$v_z^{t+\Delta t} = \sqrt{\frac{k_BT_w}{m}}v_M, \tag{6}$$

where $\widehat{n}_w$ is a unit vector directed from the wall to the bulk, v_M is a Maxwellian (with its variance corresponding to the wall temperature T_w and a mean corresponding to the wall velocity which is zero for stationary walls), and v_{BM} represents a "biased" Maxwell distribution (or a Rayleigh probability distribution [23]). The second term on the right-hand side of Eq. (4) embodies the fact that the x component of the particle velocity is accelerated (due to gravity directed along the x axis) during the free-flight time (t_{post}) between two collisions.

In the mixed thermal-wall model, α is called the ("tangential momentum") accommodation coefficient, with

$$\alpha = \begin{cases} 1 & \text{(diffuse collision)} \\ 0 & \text{(specular collision)} \end{cases} \tag{7}$$

corresponding to the limiting cases of fully diffuse and specular walls, respectively; it also represents two limiting cases of finite and zero wall friction (resistance offered by the wall to fluid flow), respectively. While the latter can be thought of an ideal wall in contact with an inviscid fluid (for which the viscous stresses are zero), resulting in full or complete slip, the former yields zero-slip velocity at walls (in the continuum limit of $\text{Kn} \to 0$).

The above "mixed" thermal-wall boundary conditions ($0 < \alpha \leqslant 1$) have frequently been used for studying flows of molecular gases [4]. It must be noted that the singular case of specular walls ($\alpha = 0$) does not truly represent a thermal wall (since the wall temperature is not specified and hence redundant); this can rather be identified with "athermal" walls that are described below.

B. Athermal walls: Tangential restitution and bulk wall roughness

For "athermal" walls [19], the temperature of wall is not specified, rather the wall is characterized by two parameters: tangential (β_w) and normal (e_w) restitution coefficients for particle-wall collisions. The particle-wall collision scheme for such athermal walls is implemented as follows [19,24,25]:

$$v_x^{t+\Delta t} = -\beta_w v_x^t + gt_{\text{post}}, \tag{8}$$

$$v_y^{t+\Delta t} = -e_w v_y^t, \tag{9}$$

$$v_z^{t+\Delta t} = -\beta_w v_z^t. \tag{10}$$

The wall-tangential restitution coefficient β_w is a measure of the bulk roughness of the wall, with

$$\beta_w = \begin{cases} -1 & \text{(smooth wall)} \\ 1 & \text{(rough wall)} \end{cases} \tag{11}$$

referring to perfectly smooth and perfectly rough limits, respectively; in Eq. (9), $e_w \leqslant 1$ is a measure of the dissipative nature of particle-wall collisions.

The primary role of β_w is to account for the momentum transfer between the fluid and the wall. In previous studies [24,25] it has been established that the perfectly rough ($\beta_w = 1$) and smooth ($\beta_w = -1$) wall conditions result in no-slip and full-slip, respectively, on the coarse-grained fluid velocity at the wall. A possible relation of β_w with an effective specularity coefficient will be discussed in Sec. IV B.

III. KNUDSEN PARADOX: ROLES OF WALL CONDITION AND INELASTICITY

Since the Poiseuille flow (see the inset of Fig. 1) has gradients only along the wall-normal (y) direction with homogeneous fields along two periodic directions (x and z), the flow domain is divided into a number of layers or bins parallel to the walls, and the coarse-grained hydrodynamic fields are calculated as described in our previous paper [20] to which the reader is referred for related details. The dimensionless mass-flow rate is calculated from

$$Q = \frac{1}{\rho_{av}\sqrt{gW}W}\int_{-W/2}^{W/2}\rho(y)u_x(y)\,dy, \tag{12}$$

which is different from that defined in Eq. (1) since the reference scales are different [and, of course, T_w is not defined for athermal walls and hence Eq. (1) cannot be used]. In the remaining figures, we nondimensionalize velocity with $\sqrt{gW}$, density with ρ_{av} and the temperature by $T_R = gW$, and use Eq. (12) to compare flow rates among different boundary conditions.

The Knudsen number (Kn) is defined as

$$\text{Kn} = \frac{\lambda_{gl}}{W}, \tag{13}$$

where $\lambda_{gl} = (\sqrt{2}\pi n_{av}d^2)^{-1}$ is the "global" mean-free path for a dilute gas (based on the average density of the gas) and W is the channel width. To carry out simulations for a range of Kn (13), we varied the mean number density (in the dilute limit $n_{av} < 0.0121$) while keeping the channel width constant at $W/d = 1800$. For the acceleration-driven Poiseuille flow, another control parameter is the dimensionless acceleration $\hat{g}$,

$$\widehat{g} = \frac{gW}{\frac{2k_BT_w}{m}}, \tag{14}$$

which measures the strength of the body force acting on a particle traveling a distance W. Since the above quantity (14) is unspecified for athermal walls, the value of g is set fixed to the same value (unless stated explicitly otherwise) while comparing results between thermal and athermal walls.

A. Thermal walls: Does the Knudsen minimum exist in a granular gas?

Although for stationary walls such as those in Poiseuille flows, the idealization of a thermal wall is not applicable for a "granular" gas (since the "granular" temperature is a by-product of the flow and cannot be *a priori* specified as an independent quantity), here we pose the following question: "If we follow a protocol as has been done for molecular gases and study the Poiseuille flow of a granular gas driven by gravity and bounded by thermal walls, does a minimum in the flow

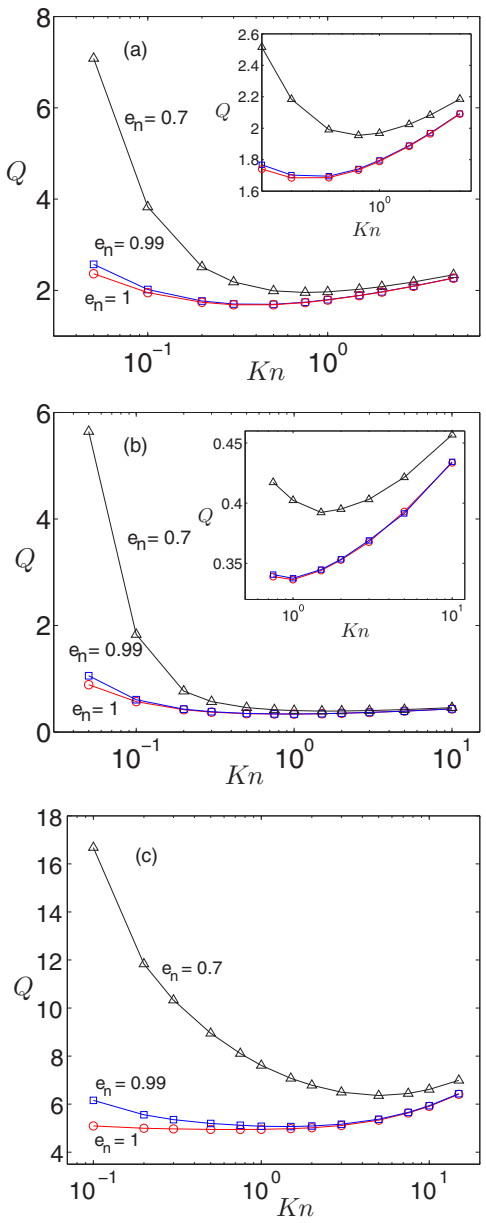

FIG. 3. Variations of the flow rate [Eq. (12)] with Knudsen number for (a, b) "diffuse" ($\alpha = 1$) and (c) "nearly specular" ($\alpha = 0.1$) thermal walls for different e_n; insets in panels (a) and (b) show a magnified version of the right "logarithmic" branch. The dimensionless acceleration is set to (a, c) $\widehat{g} = 9.3$ ($g = 0.01$), and (b) $\widehat{g} = 0.05$ ($g = 0.000053$).

rate at finite Kn occur as in Fig. 1"? The answer seems to be positive as confirmed in our recent work [20], where we used fully "diffuse" ($\alpha = 1$) thermal-wall conditions.

Figure 3(a) shows the variations of Q [Eq. (12)] with Kn for three values of restitution coefficient $e_n = 1$, 0.99, and 0.7 with diffuse ($\alpha = 1$) thermal walls; the acceleration is set to $g = 0.01$, which corresponds to a dimensionless acceleration of $\widehat{g} \sim 9.3$ with $T_w = 1$. Each flow-rate curve remains nonmonotonic with Knudsen number, and a minimum in the flow rate occurs at finite Kn $\sim O(1)$ for all e_n along with a loglike increase of Q for sufficiently large values of Kn. These overall features remain intact at different values of $\widehat{g}$ [see panel (b) for $\widehat{g} = 0.05$, as well as Appendix A] and at different values of α [see panel (c) for $\alpha = 0.1$, representing "nearly specular" thermal walls]. Note that the effect of specular particle-wall collisions ($\alpha < 1$) is to increase the wall slip and thereby increasing the mass-flow rate [26,27]; this holds also in the presence of inelastic dissipation as can be seen by comparing Q curves for $e_n = 0.7$ between Figs. 3(a) and 3(c).

In the continuum limit of small Knudsen numbers (Kn $\sim$ 0), the presence of inelastic dissipation leads to clustering of particles along the transverse or gradient direction (in unidirectional flows like Poiseuille flow) wherein the particles migrate to the region of low shear (around channel center $y = 0$), resulting in inhomogeneous density profiles with a density peak at $y = 0$; this is dubbed "dissipation-induced clustering" [19]. This has two consequences with decreasing e_n: (1) the center-line velocity increases and (2) the wall region becomes more dilute and hence rarefied, resulting in an increased slip velocity. Both effects collectively lead to an increased mass-flow rate with decreasing e_n at a given value of Kn, thus explaining the flow-rate curves for different e_n (at Kn $\sim$ 0) in all panels in Fig. 3.

Another interesting feature in Figs. 3(a) and 3(b) is that the location of $Q_{\min}$ shifts to larger values of Kn with decreasing e_n. The delay in the appearance for $Q_{\min}$ with decreasing e_n is possibly due to a competition between the "dissipation-induced clustering" and the "rarefaction-induced declustering" of particles along the transverse or gradient direction. The latter effect becomes dominant at large values of Kn, since the density profile tends to become flatter with lesser number of particle-particle collisions within the bulk as Kn is increased. While the degree of dissipation-induced clustering increases (i.e., the density contrast between the channel center and the wall region is enhanced) with decreasing e_n, the rarefaction-induced declustering is almost independent of e_n; therefore more rarefaction (i.e., larger Kn) would be needed to homogenize an inhomogeneous density field at lower values of e_n.

Overall, the present DSMC results (Fig. 3) along with those in Ref. [20] establish that inelastic dissipation does not prevent a minimum in the flow rate at finite Kn and the flow rate increases at sufficiently large values of Kn if the walls are treated as "thermal walls" (irrespective of whether the particle-wall collisions are diffuse or mixed diffuse-specular). This conclusion holds also for a dense granular Poiseuille flow [28] in contact with thermal walls.

B. Role of athermal rough or smooth walls

For "athermal-wall" conditions (Sec. II B), the present results based on DSMC simulations are summarized in Fig. 4(a) as a phase diagram in the $(\beta_w, 1 - e_n)$ plane. Inside the hatched region, the flow rate shows a nonmonotonic variation with Kn, exhibiting local minimum and maximum, such as that in the inset of Fig. 4(a) as well as in Fig. 2. The broken line marked by squares in Fig. 4(a) represents the zero loci of the quantity

$$\triangle Q = Q_{\max}(\mathrm{Kn} \neq 0) - Q_{\min}, \tag{15}$$

indicating that the flow rate in the white region of Fig 4(a) is a monotonically decreasing function of Kn. Figure 4(a) was

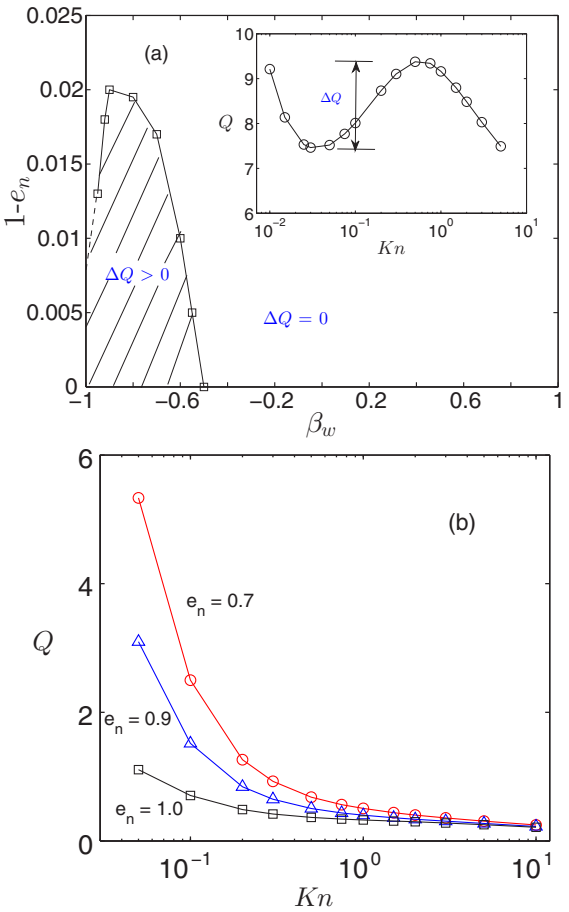

FIG. 4. (a) Phase diagram in the $(\beta_w, 1-e_n)$ plane delineating the regions of monotonic ($\triangle Q = 0$, white region) and nonmonotonic ($\triangle Q > 0$, hatched region) flow rates. β_w is a measure of the bulk roughness of the walls, with -1 and 1 representing the limiting cases of perfectly smooth and rough walls, respectively; see Sec. II B for details on boundary conditions. Inset shows the variation of the flow rate with Kn for smooth walls ($\beta_w = -0.9$), with a restitution coefficient of $e_n = 0.999$; see also Fig. 2. (b) Dimensionless flow rate [Eq. (12)] versus Knudsen number for different e_n in channels with rough walls $\beta_w = 0.9$. The dimensional acceleration is set to $g = 0.01$ for all cases.

constructed by carrying out simulations for the whole range of $\beta_w \in (-1,1)$ and thereafter measuring and plotting the zero contour of $\triangle Q$ [Eq. 15]. The overall shape of the phase diagram in Fig. 4 looks similar to Fig. 4(c) of Alam *et al.* [19] who employed a MD method to simulate the same dilute granular Poiseuille flow (with athermal walls); this also confirms the robustness of flow-rate results based on two different numerical techniques (DSMC and MD).

Focusing on the hatched region of the phase space in Fig. 4(a), the variations of the flow rate with Kn are shown in Fig. 2 (the main panel and its inset) for a wall roughness of $\beta_w = -0.9$ (nearly smooth walls). The main panel of Fig. 2 confirms that the flow rate does indeed initially decrease to a local minimum ($Q_{\min}$) and then increases to a maximum ($Q_{\max}$) beyond which it starts to decrease again when the particle collision are quasielastic ($e_n \leqslant 0.99$); for more dissipative collisions ($e = 0.9, 0.7$; see the inset of Fig. 2); however, the flow rate decreases monotonically with increasing Kn. Typical results for rough walls are shown in Fig. 4(b) for a wall roughness of $\beta_w = 0.9$; the flow rate is found to decrease monotonically with Kn at any value of e_n for this value of β_w.

The thermal-wall results presented in Fig. 3 are at odds with those with athermal walls (Figs. 4 and 2) on several counts: (1) for athemal walls the Knudsen minimum is absent for a granular gas for $e_n < 0.98$ (irrespective of wall roughness), (2) the flow rate decreases at sufficiently large values of Kn, and (3) even in the limit of elastic particle collisions [$e_n = 1$, see the horizontal axis in the phase diagram in Fig. 4(a)] the flow-rate variation with athermal walls is completely different from that of a molecular gas in contact with thermal walls. The second observation (2) implies that the flow rate increases or decreases in the free-molecular limit (Kn $\to \infty$) if the walls are thermal or athermal, respectively. Observation (3) implies that the elastic limit ($e_n \to 1$) of Poiseuille flow in contact with athermal walls might be singular. All three observations are at odds with what is well known about the century-old Knudsen paradox. Nevertheless it is clear from Figs. 3 and 4 that the wall conditions being thermal or athermal are responsible for the observed differences on the variations of the flow rate with the Knudsen number.

The way in which the thermal and athermal walls can affect the bulk properties like the mass-flow rate (at large values of Kn) remains to be clarified. This brings us to the central question: What is the mechanistic origin of the logarithmic branch [Eq. (3)] of the flow rate at Kn $\gg 1$? The remaining part of this paper addresses these two questions.

C. Connection with no-flux and adiabatic walls

Returning to collision rules [Eqs. (8)–(10)] for athermal walls, we note that in the limits of perfectly smooth and rough walls ($\beta_w \to \pm 1$) the kinetic energy of incident particles remain unchanged upon collision with walls (if the normal restitution coefficient for particle-wall collisions is $e_w = 1$); hence the athermal walls with $\beta_w \to \pm 1$ and $e_w = 1$ can be considered as "adiabatic" (see Appendix B). To establish the above link, we consider another class of athermal walls for which the reflection rule for particle-wall collisions are taken as

$$v_x^{t+\Delta t} = \sqrt{\frac{k_B T_{fw}}{m}} v_M + g t_{\text{post}}, \tag{16}$$

$$v_y^{t+\Delta t} = -v_y^t, \tag{17}$$

$$v_z^{t+\Delta t} = \sqrt{\frac{k_B T_{fw}}{m}} v_M. \tag{18}$$

This implies that while in the wall-normal direction the particle velocity reverses its direction upon collision with the wall, in the tangential directions (x and z) the particle forgets its incoming velocity and is reflected back with tangential velocity components v_x and v_z that are taken from the Maxwell distribution v_M with zero mean and a variance corresponding to T_{fw}

The crucial difference of Eqs. (16)–(18) with thermal-wall conditions (4)–(6) is that the variance of v_M in the former corresponds to a Maxwellian distribution at the temperature

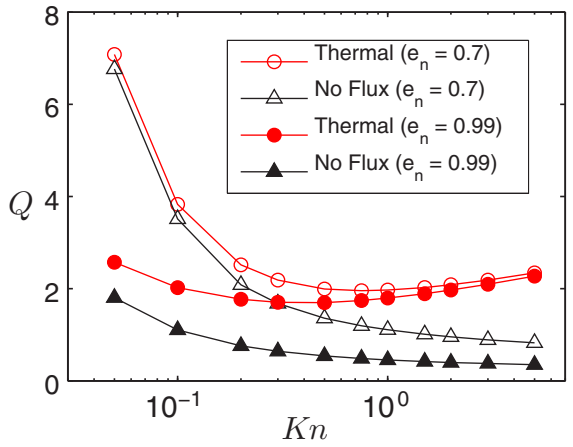

FIG. 5. Dimensionless flow rate [Eq. (12)] versus Knudsen number with "diffuse" ($\alpha = 1$) thermal (open and filled circles) and adiabatic or no-flux (open and filled triangles) walls. The filled and open symbols refer to restitution coefficients of $e_n = 0.99$ and 0.7, respectively; for both thermal and athermal walls the "dimensional" acceleration is set to $g = 0.01$.

T_{fw} of the fluid adjacent to the wall (i.e., T_{fw} is dubbed the "fluid-wall" temperature; see Appendix C for definitions of related hydrodynamic quantities extrapolated to walls). We demonstrate in Appendix B that the above wall conditions in Eqs. (16)–(18) correspond to "zero" flux of fluctuation energy at the wall ($y = \pm 1/2$) in the continuum limit of Kn $\to 0$; these are dubbed "*no-flux or adiabatic*" wall conditions.

Figure 5 compares the flow-rate variations for "adiabatic" walls (denoted by open and filled triangles) with the same for thermal walls (open and filled circles) for two representative values of restitution coefficient ($e_n = 0.99$ and 0.7). It is clear that the flow rate decays monotonically with increasing Kn when the wall conditions are adiabatic [Eqs. (16)–(18)] in contrast to the well-known slow logarithmic increase for thermal walls. Moreover, the limiting case of $e_n \to 1$ with adiabatic walls (filled triangles in Fig. 5) does not have the increasing Q branch at large Kn, indicating that even a molecular gas ($e_n = 1$) in contact with adiabatic walls would not display a flow-rate minimum at a finite Knudsen number. Collectively, these results drive home the point made in the previous section: *the absence or presence of Knudsen minimum in the Poiseuille flow of a molecular or granular gas is primarily governed by the type of wall-particle interaction*.

For both athermal and adiabatic walls, the wall temperature is not prespecified, which sets them apart from thermal walls. Moreover, the perfectly rough ($\beta_w = 1$) and smooth ($\beta_w = -1$) limits of athermal walls correspond to zero flux of fluctuation energy (see Fig. 12 in Appendix B), and hence the athermal walls are closely related to adiabatic walls for which we did not find any evidence of a Knudsen minimum.

IV. WHY ARE ATHERMAL AND THERMAL WALLS SO DIFFERENT?

It may be noted that for the Poiseuille flow in contact with thermal walls, the walls play an active role in equilibrating the system that gains energy due to shear provided by the body force. On the other hand, the adiabatic walls are devoid of such an energy exchange mechanism in the continuum limit (Kn $\to 0$). It is interesting to find the impact of different wall conditions on hydrodynamic profiles, especially on the slip velocity since the latter determines the average momentum flux transferred to the wall and thereby influences the mass-flow rate behavior.

A. Wall conditions and hydrodynamic fields

Figure 6 compares the profiles of (a, b) bulk velocity, (c, d) density, and (e, f) the momentum flux for three different wall conditions; the red solid, blue dashed, and black dotted lines correspond to thermal ($\alpha = 1$, i.e., fully diffuse), athermal ($\beta_w = 0.9$, i.e., nearly perfect rough wall), and adiabatic walls, respectively, for a restitution coefficient of $e_n = 0.7$. The panels on the left (a, c, e) and right (b, d, f) columns refer to results for Knudsen numbers of Kn $= 0.05$ and Kn $= 1$, respectively. Although the overall shapes of velocity profiles for three wall conditions look similar at small and large Kn [panels (a) and(b)], there are noticeable differences with regard to center-line ($y = 0$) and slip (at $y = \pm 1/2$) velocities: (1) the center-line velocity is largest, least and intermediate for thermal, athermal, and adiabatic walls, respectively, at both Kn $= 0.05$ and 1; (2) while the above trend holds for the slip velocity too at Kn $= 1$, at Kn $= 0.05$ the slip is maximum for adiabatic walls and least for athermal walls. Panels (c) and (d) indicate that the density profiles for athermal and adiabatic walls are almost indistinguishable from each other for both Kn $= 0.05$ and 1, with the maximum and minimum in density occurring at $y = 0$ and $y = \pm 1/2$, respectively. In contrast, for thermal walls there is a local density maximum at walls for Kn $= 0.05$ [panel (c)] that becomes a global maximum (with minimum density at $y = 0$) at higher values of Kn $= 1$ (panel (d)].

The sensitivity of the mass-flow rate (Q) with wall types can be guessed from the momentum-flux (ρU_x) profiles shown in Figs. 6(e) and 6(f). We find that while the mass-flow rate is relatively insensitive to wall conditions at small Knudsen number [Kn $= 0.05$, panel (e)], there is a multifold increase in Q at Kn $= 1$ when athermal walls are replaced by thermal walls; in particular, at large values of Kn, we found

$$Q_{\text{thermal}} > Q_{\text{adiabatic}} > Q_{\text{athermal}}. \tag{19}$$

This trend is conceivable since the particle-wall collisions would dictate the bulk behavior of flow at large Kn, and the walls being thermal or athermal are therefore felt across the channel cross section at Kn $\gg 1$.

B. Relation between athermal and thermal walls: Effective specularity coefficient and slip velocity

For athermal walls, the primary role of bulk-roughness parameter β_w is to account for the momentum transfer between the fluid and the wall. In previous studies [19,25] it has been established that the perfectly rough ($\beta_w = 1$) and smooth ($\beta_w = -1$) wall conditions results in zero-slip (i.e., $u_s = u_{fw} - u_w \approx 0$) and full-slip ($u_s \approx u_0 = u(y = 0)$) velocity, respectively (see Appendix C for the definitions of slip fields). This suggests that the bulk wall roughness β_w can be identified

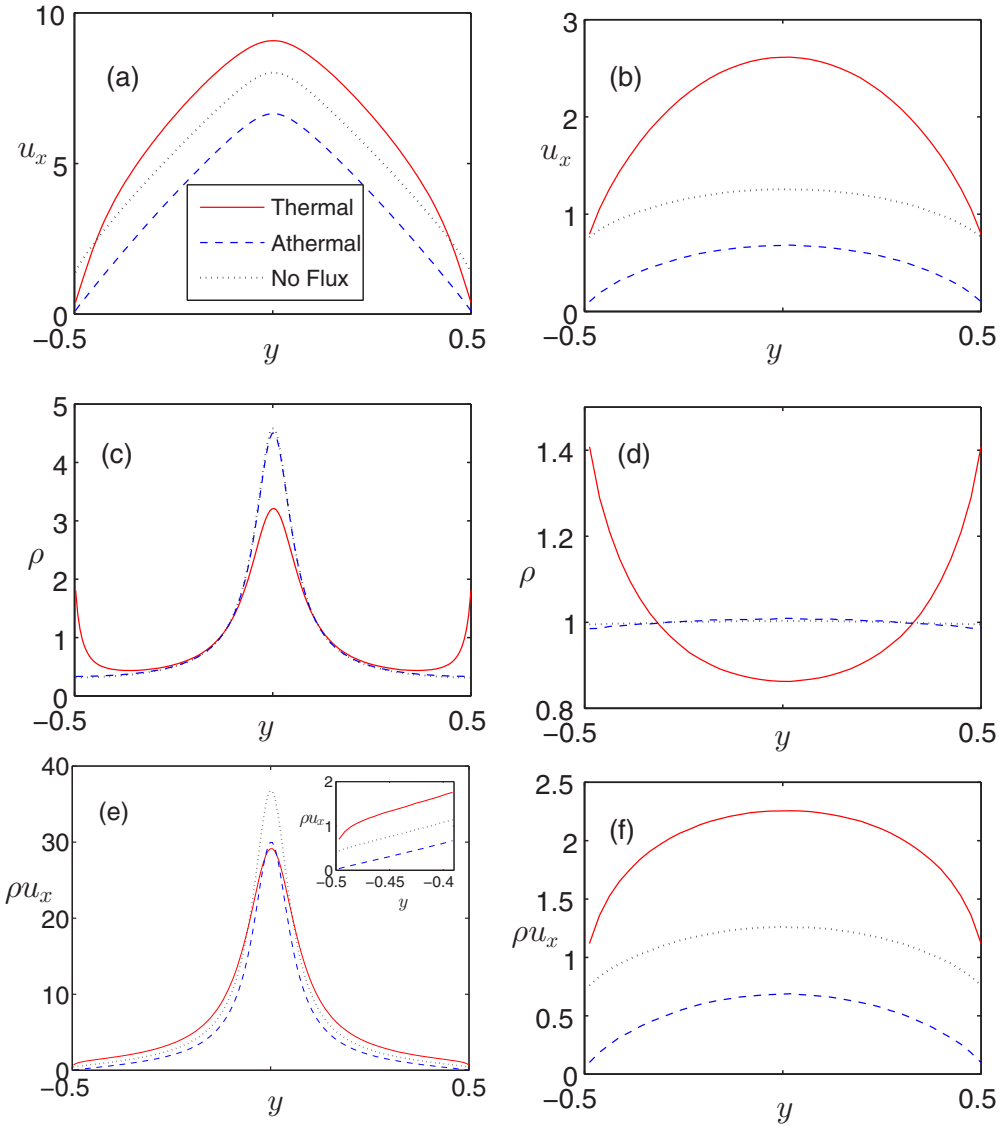

FIG. 6. Comparisons of (a, b) streamwise velocity, (c, d) density, and (e, f) momentum flux among different wall conditions: thermal (red solid line, $\alpha = 1$), athermal (blue dashed line, $\beta_w = 0.9$), and adiabatic (black dotted line); the inset in panel (e) is a zoom of the lower left corner of the same plot. The Knudsen number is Kn $= 0.05$ (left panels) and Kn $= 1$ (right panels). The restitution coefficient is $e_n = 0.7$, and the dimensional acceleration $g = 0.01$.

with an "effective" momentum-accommodation coefficient:

$$\alpha_{\text{eff}} = \frac{(1+\beta_w)}{2}. \tag{20}$$

According to this relation, the perfectly rough wall ($\beta_w = 1$) may be regarded as an effective *diffuse wall* ($\alpha_{\text{eff}} = 1$), resulting in zero-slip condition at walls, but the perfectly smooth wall ($\beta_w = -1$) is tied to the *specular wall* condition ($\alpha_{\text{eff}} = 0$), resulting in almost complete slip with a pluglike velocity profile.

The above relation (20) seems to hold in the granular Poiseuille flow [see Fig. 7(a)], which displays the variations of the dimensionless slip velocity u_s (normalized by gW) with α_{eff} for two values of restitution coefficient ($e_n = 1$ and 0.7, denoted by open and filled triangles, respectively) at Kn $=$ 0.05; the related results for thermal walls are also superimposed (denoted by open and filled circles) on the same figure. Of course, there are some quantitative differences between the slip velocities obtained using thermal and athermal walls (especially at $\alpha_{\text{eff}} \sim 1$) as well as at large Knudsen number Kn $= 1$; see Fig. 7(b). Overall, the slip velocity for athermal walls can be obtained approximately from those for thermal walls with an "effective" specularity coefficient ($\alpha = \alpha_{\text{eff}}$) if the Knudsen number is small.

On the other hand, the near-wall density ρ_{fw} (see Appendix A for its definition) can vary significantly depending on whether the walls are thermal or athermal; see Figs. 7(c) and 7(d) for Kn $= 0.05$ and 1, respectively. This density variation results in a very large change for overall momentum transfer to thermal and athermal walls,

$$M_w = \rho_{fw} u_s \equiv \rho_{fw}(u_{fw} - u_w), \tag{21}$$

as seen in Figs. 7(e) and 7(f) for Kn $= 0.05$ and Kn $= 1$, respectively. It is clear that the momentum transfer to athermal

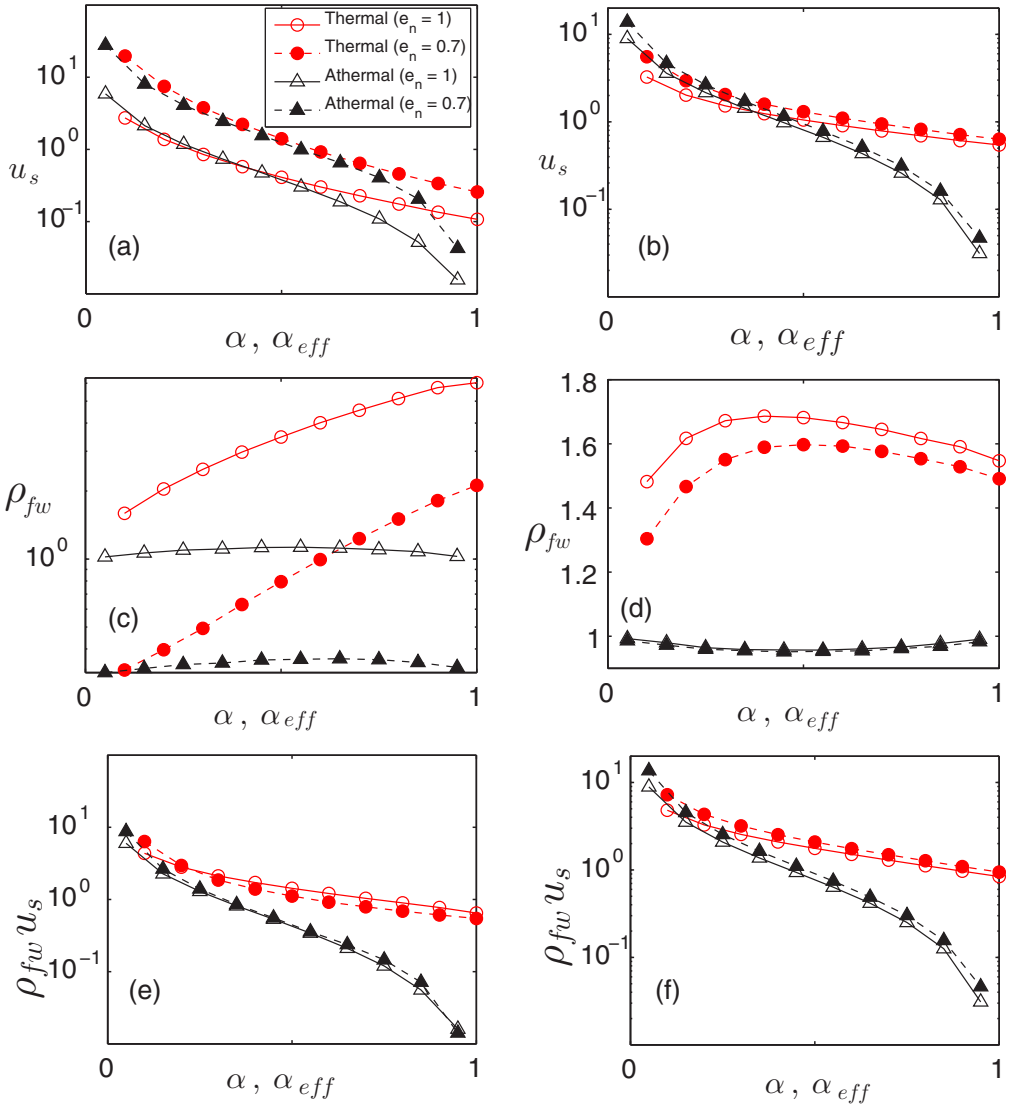

FIG. 7. Variations of (a, b) slip velocity, (c, d) wall density, and (e, f) excess momentum at wall with α (thermal wall, denoted by circles) and $\alpha_{\text{eff}} = (1 + \beta_w)/2$ (athermal wall, denoted by triangles) for two values of the global Knudsen number Kn = 0.05 (left panels) and (b) 1.0 (right panels). Open and filled symbols refer to $e_n = 1$ and 0.7, respectively, and the dimensionless acceleration is $\widehat{g} = 9.3$.

walls is lower than that to thermal walls, except for $\alpha < 0.15$ [that corresponds to nearly smooth walls, $\beta_w \to -1$, see Eq. (20)], and the difference increases as the walls are made rougher ($\beta_w \to 1$).

The latter finding holds at any e_n and Kn as confirmed in Fig. 8. It is seen that M_w can differ by two orders of magnitude between very rough ($\alpha_{\text{eff}} = 0.95$. i.e., $\beta_w = 0.9$) athermal walls and nearly diffuse ($\alpha = 0.95$) thermal walls. Such large differences in momentum transfer seem to be responsible for the continual decrease of the flow rate with Kn for rough athermal walls ($\beta_w > -0.8$).

Focusing now on "nearly smooth" ($\beta_w \to -1$) athermal walls, we show the variations of the center-line velocity (u_0) and the slip velocity (u_s) with Knudsen number in Fig. 9(a) for a wall roughness of $\beta_w = -0.8$ (i.e., $\alpha_{\text{eff}} = 0.1$). It is seen that the Kn variation of u_0 mirrors that for the flow rate; on the other hand, the slip velocity increases with Kn up to a value of Kn = 0(1) and decreases thereafter, closely following the curve of u_0. These results should be contrasted with those in Fig. 9(b) for the analogous case of "nearly specular" thermal walls ($\alpha = 0.1$). For this case too, the Kn variation of center-line velocity (u_0) follows that of its flow rate Q, with a logarithmic increase at Kn $\gg 1$. The slip velocity is found to increase monotonically with increasing Kn, and both u_s and u_0 closely follow each other at Kn $\gg 1$ with logarithmic increase. For these two cases, the momentum transfer to walls (M_w) is compared in Fig. 9(c). It is clear that the nonmonotonic variation of slip velocity with Kn leads to a similar variation of the momentum transfer to walls M_w, resulting in the decrease of M_w at Kn $\gg 1$ for athermal walls. On the other hand, both u_s and M_w continue to increase with Kn for the analogous case of nearly specular thermal walls as is evident from Figs. 9(a) and 9(c) [lines marked by circles]; these overall findings on the momentum transfer (M_w) to "specular" thermal walls ($\alpha \sim 0$) also hold at any value of acceleration; see Fig. 10. [Note that M_w, u_s, and Q have been nondimensionlized via acceleration

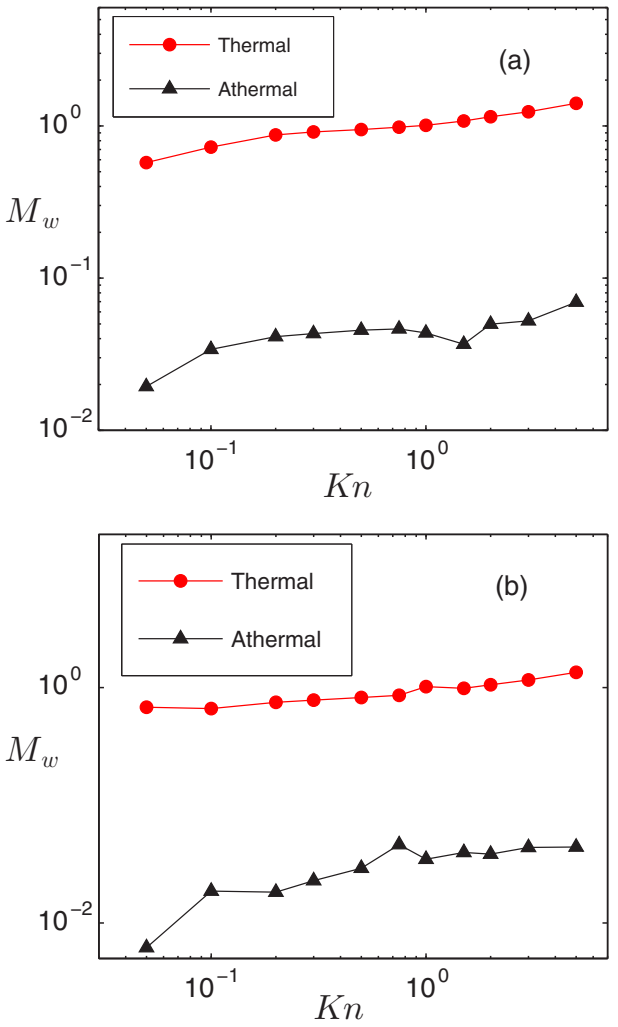

FIG. 8. Variations of excess momentum at wall ($M_w = \rho_{fw} u_s$) with Knudsen number for both thermal and athermal walls ($\alpha = 0.95 = \alpha_{\text{eff}}$) with restitution coefficient of (a) $e_n = 0.7$ and (b) $e_n = 1.0$. The dimensionless acceleration is $\widehat{g} = 9.3$.

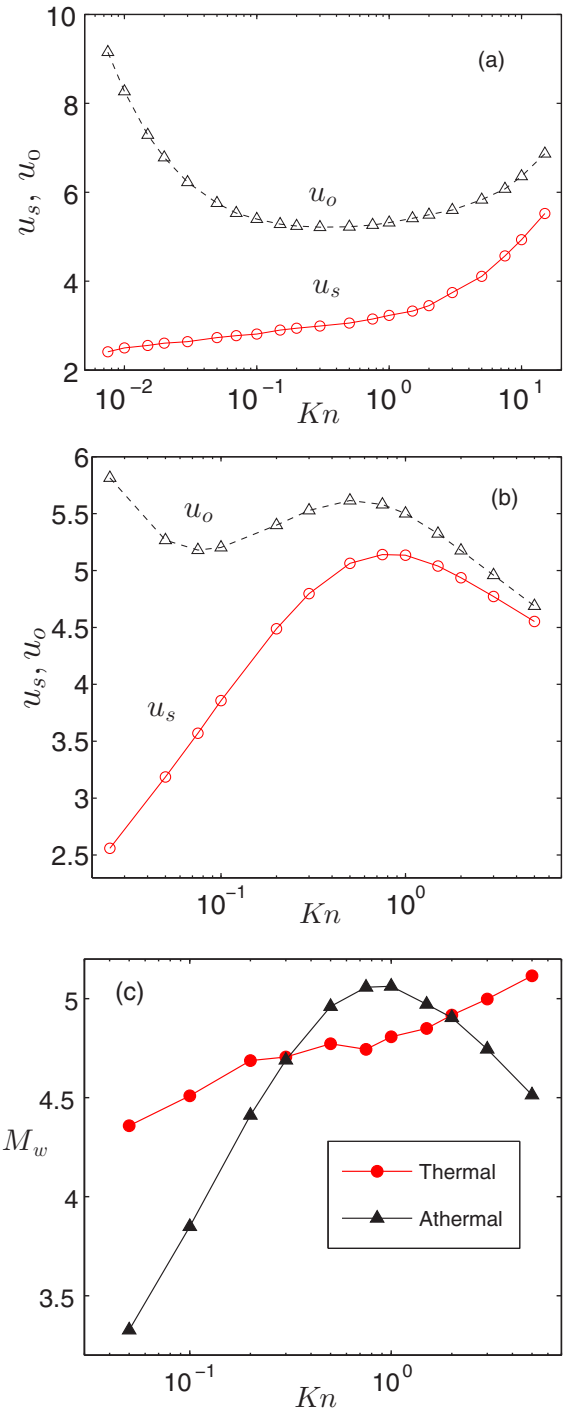

FIG. 9. Variations of slip velocity u_s (circles) and center-line velocity u_0 (triangles) with Kn for (a) thermal walls ($\alpha = 0.1$, nearly specular) and (b) "smooth" athermal walls ($\beta_w = -0.8$, i.e., $\alpha_{\text{eff}} = 0.1$). (c) Variations of excess momentum at wall ($M_w = \rho_{fw} u_s$) with Kn for thermal ($\alpha = 0.1$, filled circles) and athermal ($\beta_w = -0.8$, filled triangles) walls. For all cases, the restitution coefficient is $e_n = 1$ and the dimensionless acceleration is $\widehat{g} = 9.3$.

(g), and these "dimensionless" quantities do not depend on acceleration for athermal walls.]

Collectively, Figs. 7(e), 7(f), 8, and 9(c) confirm that the momentum transfer to walls at Kn $\gg 1$ is much lower for athermal walls (irrespective of smooth or rough walls) compared to thermal walls (lower by at least an order of magnitude), which, in turn, is responsible for the continual decrease of the flow rate with increasing Kn (and hence the absence of a Knudsen minimum) for athermal walls.

C. Effective boundary condition on slip velocity

Last, we discuss the possibility of characterizing athermal walls in terms of slip boundary conditions: whether the slip velocity for athermal walls [Figs. 7(a) and 7(b)] can be approximated by that for "thermal walls" with an effective specularity coefficient [$\alpha = \alpha_{\text{eff}}$, Eq. (20)].

For a granular gas, the first-order slip boundary condition with "diffusely" reflecting ($\alpha = 1$) wall has been derived by Goldhirsch [29]:

$$u_s = c_1 \lambda \frac{du}{dy}, \tag{22}$$

$$c_1 = 0.728 + 0.13\left(1 - e_n^2\right), \tag{23}$$

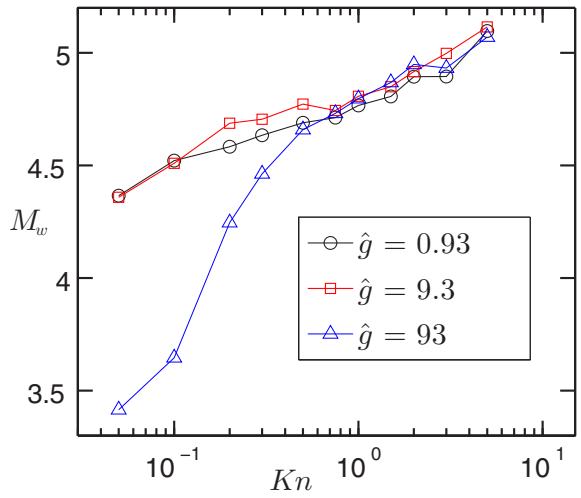

FIG. 10. Effect of dimensionless acceleration $\widehat{g}$ on the momentum transfer to walls M_w for nearly specular ($\alpha = 0.1$) thermal walls with $e_n = 1$

where λ is the "local" mean-free path (near the wall $y = \pm 1/2$). The related boundary condition for a "diffuse-specular" wall (with a specularity coefficient of $0 < \alpha \leqslant 1$) can be put into dimensionless form as follows:

$$\rho_{wf} u_s = \frac{c_1}{\alpha} \mathrm{Kn} \left(\frac{du}{dy} \right)_{fw} + \mathrm{HOT} \equiv M_w, \tag{24}$$

where $\mathrm{Kn} = (\sqrt{2}\pi n_{av} d^2)^{-1}/W$ is the global or average Knudsen number as defined in Eq. (13) and HOT refers to higher-order corrections.

According to Eq. (24), a lower value for M_w (for given Kn, α, and e_n) would imply a lower value for the velocity gradient at wall; this lower velocity gradient would persist in the bulk too if $\mathrm{Kn} \sim O(1)$, which in turn would also reduce the center-line velocity in the channel; this is evident from Fig. 6(b) by comparing the red solid and blue dashed lines for thermal and athermal walls, respectively. The combined effect would be a net decrease in the mass-flow rate for athermal walls in comparison to thermal walls at large Kn [Fig. 6(f)]. At smaller values of $\mathrm{Kn} \sim 0$, however, the above arguments hold only near the wall, and the overall flow rate would not be much affected as seen in Fig. 6(e).

The above arguments suggest that the Maxwell-type slip boundary condition [Eq. (24)] can be used for athermal walls at small values of Kn; also, the higher-order gradient terms of hydrodynamic fields need to be added on the right-hand side of (24) for its validity at larger Kn [4,5]. Regarding the temperature boundary condition, our results in Appendix B suggest the specification of heat flux at athermal walls:

$$\mathbf{n}_w \cdot \mathbf{q} = \mathbf{u}_s \cdot \mathbf{M}_w - \mathcal{D}_w, \tag{25}$$

where $\mathbf{M}_w$ is the tangential momentum flux due to particle-wall collisions, $\mathbf{u}_s$ is the slip velocity, $\mathbf{n}_w$ is the unit normal vector from the wall to the fluid, and $\mathcal{D}_w \sim (1 - e_w^2)$ is the average energy loss (per unit area) due to particle-wall collisions (e_w is the restitution coefficient for particle-wall collisions, which is set to unity in present simulations). It is noteworthy that the flux-type boundary condition on temperature [Eq. (25)] is commonly being used in granular fluids [30,31], and the present work therefore reconfirms the validity of such boundary conditions.

V. CONCLUSIONS

The DSMC simulation of the inelastic Boltzmann equation for the gravity-driven Poiseuille flow of an inelastic granular gas confirmed that the Knudsen paradox or Knudsen minimum effect survives in a granular gas ($e_n < 1$) if the walls are treated as *thermal walls* with a prespecified wall temperature [20]; this holds irrespectively of the particle-wall collisions being diffuse or mixed diffuse-specular. This is in contrast to previous molecular dynamics simulations [19] of the same system (but in channels bounded by smooth or rough walls) that showed that the flow rate at sufficiently large values of Kn always decreases with increasing Kn irrespectively of wall roughness, and hence the Knudsen mimimum does not exist for a granular gas.

The above conundrum has been resolved by distinguishing between "thermal" and "athermal" walls, with the latter being characterized by a wall-roughness parameter (β_w) that takes values between 1 and -1 for perfectly rough and smooth walls, respectively; the primary role of β_w is to transfer momentum between fluid and the athermal wall. Implementing athermal-wall conditions in DSMC simulation, it is shown that the origin of Knudsen paradox is tied to the differences in wall conditions for both molecular and granular gases, and the inelastic nature of particle collisions ($e < 1$) plays only a subdominant role in the origin of the Knudsen paradox. It is further demonstrated that the adiabatic wall conditions do not admit the Knudsen minimum in the flow rate.

We showed that the presence or absence of the Knudsen minimum is tied to the amount of the momentum transfer to walls, which surprisingly depends on the types of chosen walls (thermal or athermal) even at large Knudsen numbers. For both molecular and granular gases, the momentum transfer to athermal walls is found to be much lower than that to thermal walls, which is directly responsible for the "anomalous" flow-rate variation with Kn in the rarefied regime. In the continuum limit of $\mathrm{Kn} \to 0$, the athermal walls are in fact closely related to adiabatic walls for which the Knudsen minimum does not exist either. The underlying mechanistic arguments lead to Maxwell's slip-boundary condition, and it is shown (Sec. IV C) that the athermal walls can be characterized in terms of an effective specularity coefficient [Eq. (24)] for a slip boundary condition; on the other hand, the flux-type boundary conditions [Eq. (25)] should be specified on temperature at athermal walls.

Overall, the present work provides a unified framework for the presence or absence of the Knudsen minimum in terms of (1) particle-wall collisions, (2) wall types (thermal or athemal, or adiabatic walls), and (3) inelasticity; the crucial roles of the particle-wall interactions and the thermal or athermal nature of walls on the well-studied Knudsen paradox have been decoded. A general conclusion of our work is that the "thermal-wall"

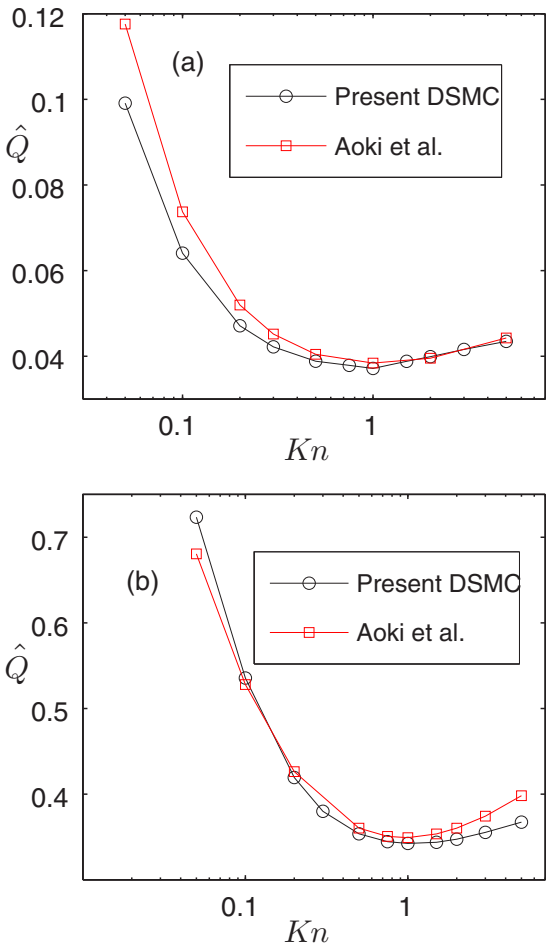

FIG. 11. Dimensionless flow rate versus Knudsen number for a molecular gas with thermal-wall conditions: (a) $\widehat{g} = 0.05$ and (b) $\widehat{g} = 0.5$. Results from Ref. [14] are also shown in panels (a) and (b) as red squares.

conditions are aphysical and inappropriate for granular gases in contact with stationary walls (such as in the context of Poiseuille flow).

ACKNOWLEDGMENTS

The research work of M.A. is partly funded by the Department of Science and Technology, Government of India (Ref. DST/INT/NL/P-03/2016).

APPENDIX A: COMPARISON WITH NUMERICAL SOLUTION OF AOKI *et al.*: MASS FLOW RATE AND THE EFFECT OF ACCELERATION STRENGTH

To assess the possible effect of acceleration on mass-flow rate, Figs. 11(a) and 11(b) compare the present DSMC data for two different values of dimensionless acceleration $\widehat{g}$ [=0.05 and 0.5, Eq. (14)] with theoretical results of Aoki *et al.* [14] who solved the Boltzmann-BGK equation numerically by a finite-difference scheme. In each panel, the dimensionless flow rate has been calculated via

$$\widehat{Q}_{ATN} = \frac{1}{2\rho_{av}\sqrt{\frac{2k_BT_w}{m}}W}\int_{-W/2}^{W/2}\rho(y)u_x(y)\,dy. \tag{A1}$$

where the suffix ATN refers to dimensionalization adopted in the work of Aoki *et al.* Both sets of data correspond to thermal-wall conditions ($T = T_w$) as discussed in Sec. II A.

Figures 11(a) and 11(b) confirm that our code is able to capture the main characteristic features of Knudsen minimum effect: the flow rate decreases with increasing Kn, reaches a minimum, and then shows a slow loglike increase. Increasing gravity [$\widehat{g} = 0.5$, panel (b)] enhances the normalized flow rate (A1), but the location of the $Q_{\min}$ appears to have shifted to a lower value of Kn ≈ 0.8 (in comparison to its location at Kn ≈ 1 with $\widehat{g} = 0.05$); this finding is similar to that of Aoki *et al.* [14]. On the other hand, the present results do not agree "quantitatively" with Aoki *et al.* for all Kn, which could be due to the underlying difference in the implementation of thermal boundary conditions. In Ref. [14] each component of the postcollisional particle velocity (after a collision with walls) is initialized by the same Maxwell distribution [see Eqs. (4)–(6)]; in present simulations, however, the velocity in the wall-normal direction is sampled from a "biased" Maxwellian [Eq. (5)]. The former boundary condition can produce certain spurious results; see Ref. [22] for further details. The latter type of thermal-wall conditions has been used in previous simulations for molecular [32] and granular gases [23].

APPENDIX B: HEAT-FLUX PROFILES FOR DIFFERENT WALLS

The heat flux (i.e., the flux of the fluctuation energy) is calculated from the following expression:

$$\mathbf{q}_\alpha(y) = \tfrac{1}{2}N_e\langle m(\mathbf{v}_\alpha - \mathbf{u}_\alpha)|\mathbf{v} - \mathbf{u}|^2\rangle_y, \tag{B1}$$

where $\mathbf{v}$ is the instantaneous particle velocity and $\mathbf{u}$ is the hydrodynamic velocity [20].

With wall conditions as in Eqs. (16)–(18), the heat-flux profiles are displayed in Fig. 12 for a Knudsen number of Kn $= 0.05$ with adiabatic [panel (a)], athermal [panel (b)], and thermal [panel (c)] walls. In each panel the solid and dashed lines correspond to normal (q_y) and tangential (q_x) components of the heat flux. It is clear that both $q_x(\pm 1/2)$ and $q_y(\pm 1/2)$ are approximately zero at Kn $= 0.05$ [panel (a)]. For the same parameter values, the heat-flux profiles for athermal walls [panel (b)] look similar to those of adiabatic walls but with a small but no-zero heat flux. In contrast, the heat-flux profiles for thermal walls [panel (c)] are vastly different with large heat flux at walls. Therefore, the thermal walls allow heat transfer (this is expected since these walls are assumed to be connected with a heat reservoir at $T = T_w$) in the limit of small Kn. On the other hand, the athermal walls behave like "adiabatic" walls in the same limit of Kn $\to 0$ since the transverse profiles of q_x and q_y look similar for both wall types. This analogy between adiabatic and athermal walls indicates that the boundary conditions on heat flux should be specified

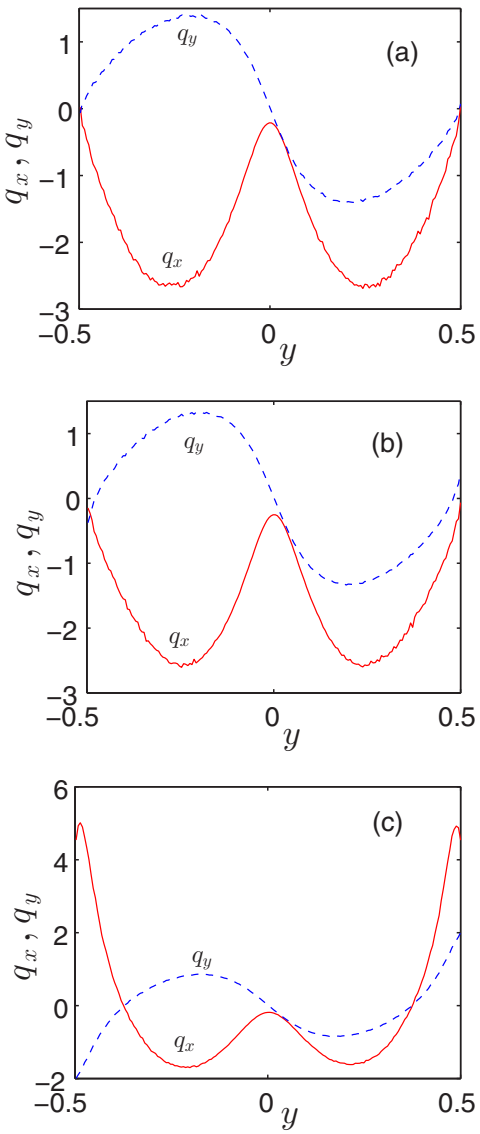

FIG. 12. Profiles of tangential (q_x, red solid line) and normal (q_y, blue dashed line) heat flux in granular Poiseuille flow in contact with (a) adiabatic, (b) athermal ($\beta_w = 0.9$), and (c) thermal ($\alpha = 1$) walls. The restitution coefficient is $e_n = 0.7$ and the global Knudsen number Kn $= 0.05$.

for athermal walls; this issue is further elaborated at the end of Sec. IV C.

Note that it is not possible to define the parameter $\widehat{g} = gW/(2k_BT_w/m)$ for simulations with adiabatic walls since the temperature of the wall is not specified *a priori*. Such walls do not allow energy exchange, and they cannot be used for molecular gas ($e = 1$) simulations without an external thermostat.

APPENDIX C: HYDRODYNAMIC FIELDS AT THE WALL

The fluid properties at the wall ($y = \pm 1/2$) are obtained by extrapolating the respective hydrodynamic profile (such as those in Fig. 6) to two walls at $y = \pm 1/2$ and then averaging its value over two walls:

$$u_{fw} = \frac{u(1/2) + u(-1/2)}{2\sqrt{gW}} \equiv u_s, \tag{C1}$$

$$T_{fw} = \frac{T(1/2) + T(-1/2)}{2gW} \equiv T_s, \tag{C2}$$

$$\rho_{fw} = \frac{\rho(1/2) + \rho(-1/2)}{2\rho_{av}}, \tag{C3}$$

where the subscript "fw" is used to denote fluid properties evaluated at the wall $y = \pm 1/2$. The first two quantities (u_{fw} and T_{fw}) are called velocity slip ($u_s = u_{fw} - u_w$) and temperature slip ($T_s = T_{fw} - T_w$), respectively, since the walls are stationary and the "granular" temperature of athermal walls is zero.

For thermal walls, the velocity slip and the near-wall fluid density are the same as above, but the temperature slip is defined as

$$T_s = \frac{[T(1/2) + T(-1/2)]}{2gW} - \frac{T_w}{gW} = T_{fw} - \frac{T_w}{gW}. \tag{C4}$$

Note that the second term on the right is zero for athermal walls ($T_w = 0$).

[1] J. C. Maxwell, On stresses in rarefied gases arising from inequalities of temperature, Philos. Trans. R. Soc. Lond. **170**, 231 (1879).

[2] M. Knudsen, Gesetze der Molekularstromung und der inneren Reibungsstromung der Gase durch Rohren, Ann. Phys. **28**, 75 (1909).

[3] M. N. Kogan, *Rarefied Gas Dynamics* (Plenum Press, New York, 1969).

[4] C. Cercignani, *Rarefied Gas Dynamics* (Cambridge University Press, Cambridge, 2000).

[5] H. Struchtrup, *Micro Flows: Fundamentals and Simulation* (Springer, Berlin, 2005).

[6] C. Cercignani and A. Daneri, Flow of a rarefied gas between two parallel plates, J. Appl. Phys. **34**, 3509 (1963).

[7] D. Burnett, The distribution velocities in a slightly nonuniform gas, Proc. Lond. Math. Soc. **39**, 385 (1935).

[8] H. Grad, On the kinetic theory of rarefied gases, Commun. Pure Appl. Maths. **2**, 331 (1949).

[9] M. Tij and A. Santos, Perturbation analysis of a stationary nonequilibrium flow generated by external force, J. Stat. Phys. **76**, 1399 (1994).

[10] M. Tij and A. Santos, Poiseuille flow in a heated granular gas, J. Stat. Phys. **117**, 901 (2004).

[11] M. M. Mansour, F. Baras, and A. L. Garcia, On the validity of hydrodynamics in plane Poiseuille flows, Physica A **240**, 255 (1997).

[12] N. G. Hadjiconstantinou, Dissipation in small-scale gaseous flows, ASME J. Heat Trans. **125**, 944 (2003).

[13] T. Ohwada, Y. Sone, and K. Aoki, Numerical analysis of the Poiseuille and thermal transpiration flows between two parallel plates on the basis of the Boltzmann equation for hard-sphere molecules, Phys. Fluids A **1**, 2042 (1989).

[14] K. Aoki, S. Takata, and T. Nakanishi, Poiseuille-type flow of a rarefied gas between two parallel plates driven by a uniform external force, Phys. Rev. E **65**, 026315 (2002).

[15] Y. Zheng, A. L. Garcia, and B. J. Alder. Comparison of kinetic theory and hydrodynamics for Poiseuille flow, J. Stat. Phys. **109**, 495 (2002).

[16] C. S. Campbell, Rapid granular flows, Annu. Rev. Fluid Mech. **22**, 57 (1990).

[17] T. Pöschel and S. Luding, *Granular Gases* (Springer, Heidelberg, 2001).

[18] I. Goldhirsch, Rapid granular flows, Annu. Rev. Fluid Mech. **35**, 267 (2003).

[19] M. Alam, A. Mahajan, and D. Shivanna, On Knudsen minimum effect and temperature bimodality in a dilute granular Poiseuille flow, J. Fluid Mech. **782**, 99 (2015).

[20] R. Gupta and M. Alam, Hydrodynamics, wall-slip, and normal-stress differences in rarefied granular Poiseuille flow, Phys. Rev. E **95**, 022903 (2017).

[21] G. A. Bird, *Molecular Gas Dynamics and the Direct Simulation Monte Carlo of Gas Flows* (Clarendon, Oxford, 1994).

[22] R. Tehver, F. Toigo, J. Koplik, and J. R. Banavar, Thermal walls in computer simulation, Phys. Rev. E **57**, R17 (1998).

[23] T. Pöschel and T. Schwager, *Computational Granular Dynamics* (Springer, Berlin, 2005).

[24] V. K. Chikkadi and M. Alam, Slip velocity and stresses in granular Poiseuille flow via event-driven simulation, Phys. Rev. E **80**, 021303 (2009).

[25] M. Alam and V. K. Chikkadi, Velocity distribution functions and correlations in granular Poiseuille flow, J. Fluid Mech. **653**, 175 (2010).

[26] C. Cercignani, M. Lampis, and S. Lorenzani, Plane Poiseuille flow with symmetric and nonsymmetric gas-wall interactions, Trans. Theory Stat. Phys. **33**, 545 (2004).

[27] Z. Gao, J. Qin, and C. Zheng, Generalized second-order slip boundary condition for nonequilibrium gas flows, Phys. Rev. E **89**, 013021 (2014).

[28] L. Wu, H. Liu, J. M. Reese, and Y. Zhang, Non-equilibrium dynamics of dense gas under tight confinement, J. Fluid Mech. **794**, 252 (2016).

[29] I. Goldhirsch, Granular gases: Probing the boundaries of hydrodynamics, in *Granular Gases*, edited by T. Pöschel and S. Luding (Springer, Berlin, Heidelberg, 2001).

[30] J. T. Jenkins and M. W. Richman, Boundary conditions for plane flows of smooth, nearly elastic, circular disks, J. Fluid Mech. **171**, 53 (1986).

[31] K. Hui, P. K. Haff, J. E. Ungar, and R. Jackson, Boundary conditions for high-shear grain flows, J. Fluid Mech. **145**, 223 (1984).

[32] F. J. Alexander and A. L. Garcia, The direct simulation Monte Carlo method, Comput. Phys. **11**, 588 (1997).